ISA Transactions 71 (2017) 563–572

Contents lists available at ScienceDirect

ISA Transactions

journal homepage: www.elsevier.com/locate/isatrans

Research article

Energy evaluation of low-level control in UAVs powered by lithium polymer battery

Daniel C. Gandolfo *, Lucio R. Salinas, Mario E. Serrano, Juan M. Toibero

Instituto de Automática (INAUT), Universidad Nacional de San Juan, CONICET, Avda. San Martín Oeste 1109, J5400ARL San Juan, Argentina

ARTICLE INFO

Article history:
Received 13 March 2017
Received in revised form
14 July 2017
Accepted 16 August 2017
Available online 1 September 2017

Keywords:
Propulsion system
Unmanned aerial vehicle
Energy savings
Battery model
State of charge
Control technique

ABSTRACT

Nowadays, the energetic cost of flying in electric-powered UAVs is one of the key challenges. The continuous evolution of electrical energy storage sources is overcome by the great amount of energy required by the propulsion system. Therefore, the on-board energy is a crucial factor that needs to be further analyzed. In this work, different control strategies applied to a generic UAV propulsion system are considered and a lithium polymer battery dynamic model is included as the propulsion system energy source. Several simulations are carried out for each control strategy, and a quantitative evaluation of the influence of each control law over the actual energy consumed by the propulsion system is reported. This energy, which is delivery by the battery, is next compared against a well-known control-effort-based index. The results and analysis suggest that conclusions regarding energy savings based on control effort signals should be drawn carefully, because they do not directly represent the actual consumed energy.

1. Introduction

Today, there is a large interest worldwide in the development of UAV (unmanned aerial vehicles) because they have proven to be effective in many civil and military applications. Most notably, electric-powered UAVs are becoming increasingly popular mainly due to the evolution of propulsion systems, improvements in energy storage technologies and small-embedded computers with high processing capacity, a significant reduction in monetary costs and positive impact on the environment. However, the on-board energy is limited and energy autonomy is nowadays one of the biggest challenges faced by these aircrafts, specially rotorcafts such as helicopters and multicopters. In the literature, it is possible to find a multidisciplinary approach oriented to improve the energetic autonomy in many type of UAVs. These approaches include aerodynamic and structural studies, materials technology, energy harvesting technologies and different guidance and control strategies.

From the control strategy point of view, there are three well-defined control levels for any aircraft, as shown in Fig. 1. Numerous control techniques and navigation strategies have been proposed by many authors for different types of UAV in order to improve, inter alia, energy autonomy. These techniques are implemented mainly in medium and high control levels.

In general, path planning control strategies (high-level control) involves multiple optimal objectives where maximal safety and minimal energy cost are the two most common objectives [1,2]. The authors in [3] propose a flatness-based flight trajectory planning/replanning strategy for a quadrotor UAV with the objective to minimize the consumed energy (among other objectives). Then, minimal-energy planning consists in minimizing an index that includes the thrust generated by each motor. In order to consider the maneuverability of the UAV, threat avoidance and fuel consumption, [4] proposes an improved A* algorithm for the UAV path planning in a 3D large-scale battlefield. The feasibility of the proposal was demonstrated through several simulation results. On the other hand, the same technique is used by [5] when planning long distance autonomous soaring trajectories for small uninhabited aerial vehicles harvesting energy from the atmosphere. In a similar way, the authors in [6] propose a unit quaternion based method to design the optimal paths with maximum sun exposure for unmanned aerial vehicles equipped with photovoltaic cells on their wings. Using chaos theory, [7] proposes a path planning by fitness-scaling adaptive chaotic particle swarm optimization, where a cost function for traveling along the trajectory is defined as a weighted sum of the threat and fuel consumption.

The mid-level control is one of the most addressed topics in UAV motion control. Several control techniques have been widely

* Corresponding author.
E-mail addresses: dgandolfo@inaut.unsj.edu.ar (D.C. Gandolfo), lsalinas@inaut.unsj.edu.ar (L.R. Salinas), serranoemanuel84@gmail.com (M.E. Serrano), mtoibero@inaut.unsj.edu.ar (J.M. Toibero).

http://dx.doi.org/10.1016/j.isatra.2017.08.010
0019-0578/

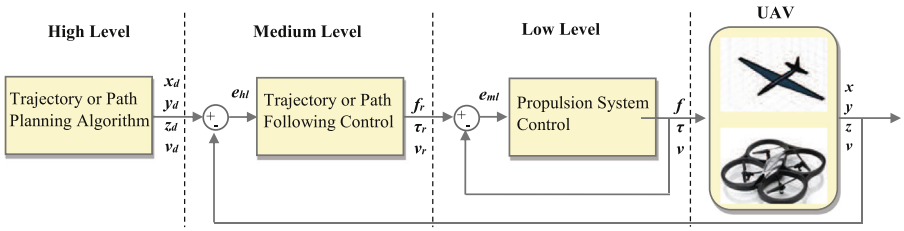

Fig. 1. UAVs hierarchical control levels.

studied and reported in the literature, such as neural networks [8,9], sliding mode control [10–12], Lyapunov theory [13–15], predictive control [16,17], state feedback control [18,19], fuzzy logic [20,21], optimal control [22,23], linear algebra theory [24,25], and a mix of them [26], among others. In most cases, the main objective is to track a desired reference, with bounded positions errors, using a stabilizing control law; but the real energy involved in the control strategy is not taken into account. In some works like [27–29], the control of the UAV is achieved by minimizing a performance index that considers control efforts among other parameters.

There is not an extensive literature on the low-level UAV control, so relevant publications are hard to find. In general, commercial off-the-shelf motor drivers use PID-based control techniques or other control type unavailable to the end user. The most commonly used controller for the propulsion system reported in the addressed literature is the PID [30,31] or PI [32,33]. In order to control a Multi-Rotor VTOL, [34] proposes three versions of PID controllers, which are evaluated and compared with each other reporting experimental results. The authors in [35] propose a classical PID tracking controller using ZieglerNichols tuning method. In [36] a quadrotor was designed considering the characteristics of high-power brushless motors and electronic speed controllers, using simple feedback loops to stabilize the platform. In [37] a hexarotor vehicle concept has been prototyped in a facecentered planar configuration with fixed-pitch/variable-speed rotors where position and attitude controllers have been successfully synthesized for the vehicle based on full state feedback control. In this case, the authors defined an analytical derivation of the static mappings between demanded control forces and torques and the required rotor thrusts. An attitude control of a Quad-Rotor Tail-Sitter VTOL UAV is presented in [38]. There, the authors argue that the altitude and attitude control performance is deteriorated by changes in battery conditions and motor load due to disturbances, hence a feedback control of the propeller revolution speed is introduced in the control system to enhance robustness against these changes. As an alternative to PID control, [39] proposes a backstepping neural adaptive control law for ducted-fan UAVs. The results indicate that the proposed control approach provides necessary stability and tracking performance; however, there is neither a comparison with other control techniques nor an evaluation of control efforts.

In the addressed literature, most advanced control techniques are implemented at medium and high control levels. The low-level control strategies use classical control theory, typically PID controllers. On the other hand, the main objective of most studies is trajectory tracking through stabilizing control laws. As for energy-saving assessments that may involve different control laws, they are usually estimated based on controls efforts. Nonetheless, there is not a clear idea of the actual energy savings due to the reduction of control actions, since the relationship between control efforts and actual energy consumption has not been clearly studied or reported. In fact, the authors in [3] state: “It is not an easy task to derive a formal equation for the energy spent during a mission and if such an equation exists, it would be nonlinear and not easy to deal with. However, it is obvious that the thrust and the consumed energy are somewhat proportional, i.e., the more thrust is generated, the more energy is consumed and vice-versa”.

In this work, four known different control strategies are applied to a generic UAV propulsion system. Low-level control was addressed because it is the least studied and the most important source of energy consumption in UAV systems.

The main contribution of this work is the inclusion of the mathematical model of the lithium polymer battery in the propulsion control scheme and the analysis of the actual energy consumed by the propulsion system under different types of control laws. Furthermore, a comparison between a well-known control-effort-based index and an index based on actual consumed energy proposed here is reported. In the addressed literature, the authors do not include the lithium polymer battery model in the control strategy in order to analyze the actual consumed energy. Even more, some of these authors draw conclusions about energy savings taking into account only a control-effort-based index which, as shown in this work, does not clearly reflect the actual energy delivered by the battery (this is a very important aspect to consider in UAV missions). These results may encourage other researchers to follow a similar approach in other control levels in UAV systems.

2. Control levels of UAVs

In general, there are three levels of control in UAVs, each one with different control techniques, as shown in Fig. 1. These control schemes usually work in coordination since most of them include model based strategies that depend on the type of UAV.

The high-level control is normally a path or trajectory planning algorithm responsible for generating a path or trajectory specified by some criteria, e.g. minimum energy, minimum time, obstacle avoidance. In any case, the reference path (x_d, y_d, z_d) and the speed at which it must be covered (v_d) are outputs of this level and inputs for the following.

In the medium-level control, two kind of control strategies are mainly used: (a) *Trajectory tracking control*, where the reference is parameterized in time (the UAV should be in certain point at certain time) and, (b) *Path following*, where the reference is not parameterized in time, and the UAV must follow the path at a given desired velocity. This control level is usually also based on the UAV mathematical model. The models most commonly used are: (a) *Kinematic model*, where the control actions are velocities that the UAV should reach to follow a desired reference; (b) *Dynamic model*, where the control actions are forces and torques applied to the UAV in order to reach the desired reference, taking into account the UAV inertial parameters.

The low-level control is basically the propulsion control system, as well as servo motors that move different parts; e.g. the flaps in fixed-wing UAVs or the swashplate in helicopters. The reference inputs for this control level are the outputs of the previous one. Thus, the thrust and torque calculated by the medium level (f_r, τ_r) should be generated by the propulsion system which basically

comprises an engine, a propeller, a dc-dc converter and a battery. Thus, to generate a given thrust, the propeller must rotate at a determined speed.

3. Low-level control scheme

In order to control the motor speed of a UAV propulsion system, four different controllers are implemented. Fig. 2 shows the complete scheme developed in Matlab/Simulink. This scheme has five well-defined blocks, which will be detailed in this section. Notice the inclusion of the lithium polymer battery model replacing the usually considered ideal source of energy.

It is worth bearing in mind that there is an energy consumption associated with the implementation of any control law in onboard computers. The more complex the calculations to obtain the control actions are, the greater will be the associated energy consumption. For this reason, simple control laws are preferred. This is usually a factor to consider in Nano-UAVs (very small size drones) where the onboard energy is extremely limited. Nevertheless, in all UAVs (and preferably in rotary-wing UAVs like helicopters) the more significant source of energy consumption is the propulsion system (motor-propeller assembly).

3.1. Propulsion system model

Normally the engine used in the propulsion of UAVs is a brushless dc motor (BLDC). BLDCs are typically permanent synchronous motors and they are well driven by dc voltage. One of the major differences between the dc motor and BLDC is that conventional dc motor has brushes which are attached to its stator while the "brushless" dc motor does not. Also, unlike the normal dc motor, the commutation of the BLDC could be done by electronic control. Numerous authors have identified and modeled the motors used in the propulsion systems as convectional dc motors [40–45]. In this paper, the model identified by [40] is adopted with their associated parameters. The dc motor coupled with a given propeller is governed by the following dynamics:

$$v_a = RI + L\frac{dI}{dt} + k_e\omega \tag{1}$$

$$K_m I = J_r\frac{d\omega}{dt} + k_r\omega^2 + C_s \tag{2}$$

It is considered a small motor with a very low inductance, then the second order dc motor dynamics may be approximated combining (1) and (2) as:

$$\dot{\omega} = bv_a - a_0 - a_1\omega - a_2\omega^2 \tag{3}$$

with $a_0 = \frac{C_s}{J_r}$, $a_1 = \frac{K_eK_m}{J_rR}$, $a_2 = \frac{K_r}{J_r}$ and $b = \frac{K_m}{J_rR}$.

The differential Eq. (3) represents the relationship between the speed ω of the motor (the variable to be controlled) and the armature voltage v_a (the control action), where R and J_r are the motor internal resistance and the rotor inertia respectively. K_e, K_m and K_r represent the electrical, mechanical and load torque constants respectively. C_s denotes the solid friction. Note that the load torque due to propeller is proportional to ω^2 and there is a drive gear reduction ratio of 6:1 between the motor axis and the propeller.

3.2. Controllers

Four controllers were considered to evaluate their performances: (1) the classical PID controller, designed to be the reference controller; (2) the Lyapunov based controller; (3) the sliding mode controller; and (4) the linear algebra based controller. The output u of each controller is the armature voltage v_a to be applied to the propulsion system.

3.2.1. PID controller

This classical controller is proposed because it is the most commonly used in this kind of low-level control stage; therefore, it is the reference controller with which to compare the others. The control law is given by (4)

$$u(t) = k_Pe(t) + k_D\frac{de(t)}{dt} + k_I\int e(t)\,dt \tag{4}$$

In this case, $e(t)$ is the velocity error $e(t) = \omega_r - \omega$ and k_P, k_D and k_I are the proportional, derivative and integral gains respectively which are adjusted for an appropriate response of the motor.

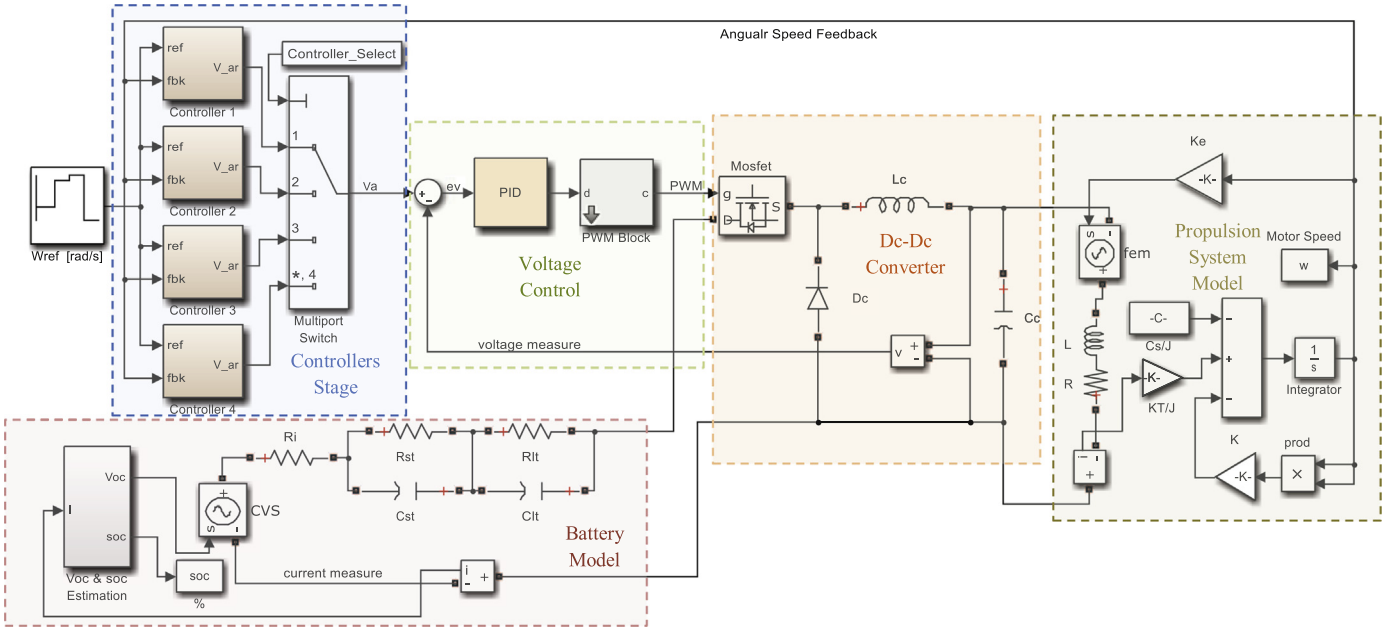

Fig. 2. Low-level control scheme including the lithium polymer battery dynamic model.

3.2.2. Lyapunov based controller

Lyapunov theory is used to make conclusions about trajectories of dynamical systems without solving the differential equation. It is a widely considered instrument that allows to design stable controllers and analyze stability of linear and nonlinear dynamic systems. Stability in the sense of Lyapunov regards the stability of solutions of differential equations near to a point of equilibrium. See [46] for details.

The equilibrium point is defined as

$$\tilde{\omega} = \omega - \omega_d = 0$$

For the proposed control action

$$u = \frac{1}{b}\left(-a_0 - a_1\omega - a_2\omega^2 - k_L\tilde{\omega}\right)$$

with $k_L > 0$ and a_0, a_1 and a_2 from (3). The closed-loop equation is

$$\dot{\omega} = b\frac{1}{b}\left(-a_0 - a_1\omega - a_2\omega^2 - k_L\tilde{\omega}\right) + a_0 + a_1\omega + a_2\omega^2 = -k_L\tilde{\omega}$$

Now, by considering the following Lyapunov candidate function

$$V = \frac{1}{2}\tilde{\omega}^2$$

The derivative along system's trajectories

$$\dot{V} = \tilde{\omega}\dot{\tilde{\omega}} = \tilde{\omega}(\dot{\omega} - \dot{\omega}_d) = \tilde{\omega}\dot{\omega} = -k_L\tilde{\omega}^2 < 0$$

This way is proved the asymptotic stability property for the equilibrium point.

3.2.3. Sliding mode controller

Sliding Mode Control (SMC) is a nonlinear control technique consisting of two parts. The first one involves the design of a sliding surface so that the sliding motion satisfies design specifications, whereas the second part is concerned with the selection of a control law that make the switching surface attractive to the system state. See [47] for details.

For the first order system, the equation of the sliding surface s is

$$s = \tilde{\omega}$$

In order to design a sliding mode controller it is next considered the time-derivative of s

$$\dot{s} = \dot{\tilde{\omega}} = \dot{\omega} - \dot{\omega}_d = \dot{\omega} = b\hat{u} + a_0 + a_1\omega + a_2\omega^2$$

with a_0, a_1 and a_2 from (3). $\hat{u}$ is the best approach to obtain $\dot{s} = 0$ provided that the value for a_2 is only approximately known, but bounded by $A_2 \geq \left|a_2 - \hat{a}_2\right|$; then

$$\hat{u} = \frac{1}{b}\left(-a_0 - a_1\omega - \hat{a}_2\omega^2\right)$$

Now, to fulfill the sliding condition it is added a discontinuous term with the $sgn(.)$ function

$$u = \hat{u} - \frac{k_s}{b}\,\mathrm{sgn}\,(s). \tag{5}$$

Hence,

$$\begin{aligned}
s\dot{s} &= s\left(bu + a_0 + a_1\omega + a_2\omega^2\right)\\
s\dot{s} &= s\left(b\left(\frac{1}{b}\left(-a_0 - a_1\omega - \hat{a}_2\omega^2 - k_s\,\mathrm{sgn}\,(s)\right)\right) + a_0 + a_1\omega + a_2\omega^2\right)\\
s\dot{s} &= s\left(\left(a_2 - \hat{a}_2\right)\omega^2 - k_s\,\mathrm{sgn}\,(s)\right) = \left(a_2 - \hat{a}_2\right)s\omega^2 - k_s\,|s|\\
s\dot{s} &\leq \left|a_2 - \hat{a}_2\right||s|\omega^2 - k_s\,|s|\\
s\dot{s} &\leq A_2\omega^2|s| - k_s\,|s|\\
s\dot{s} &\leq -\eta|s|
\end{aligned}$$

The sliding condition will be satisfied only for

$$k_s \geq A_2\omega^2$$

Finally, in order to reduce the chattering effect, the sign function is replaced by the saturation function in (5)

$$u = \hat{u} - \frac{k_s}{b}\,\mathrm{sat}\left(\frac{s}{\phi}\right)$$

where sat(.) is the saturation function which replaces the on-off behavior proper of the $sgn(.)$ function by a linear behavior in $[-\phi, \phi]$, both k_s and ϕ are positive design constants.

3.2.4. Linear algebra based controller

This is a tracking control technique based on linear algebra theory to achieve an easily implemented control law and the details can be found in [24]. Discretizing Eq. (3) one get:

$$\omega(j+1) = \left(bu(j) - a_0 - a_1\omega(j) - a_2\omega^2(j)\right)T_s + \omega(j) \tag{6}$$

where $\omega(j)$ represent the speed in the actual time instant and $\omega(j+1)$ one sample time T_s later. If $\omega(j+1)$ is replaced by the desired speed reference ω_r, the necessary control action can be derived from (6) as follows

$$u(j) = \frac{1}{b}\left(\frac{\omega_r(j) - K_a\left(\omega_r(j-(1) - \omega_r(j)\right) - \omega(j)}{T_s} + a_0 + a_1\omega(j) + a_2\omega^2(j)\right) \tag{7}$$

In the above equation K_a is introduced as a parameter design in order for the tracking error to tend to zero smoothly (for details see Section 4 of [24]).

3.3. PWM voltage controller and dc-dc converter

To apply the armature voltage v_a, calculated at the controller's stage, at the motor terminals, a dc-dc converter is used along with a voltage control block. The dc-dc converter is a switching device that transforms the fixed dc input from the battery to a variable dc output voltage which is directly applied to the motor terminals. The converter is controlled by a PID-PWM controller that allows its output voltage to follow the given desired voltage v_a.

The PID-PWM controller transforms the voltage error signal into a constant frequency and variable pulse width signal (PWM) which is applied to the base of a MOSFET transistor. This way, the dc-dc converter and its voltage control materializes the control action calculated by the controller's stage. The dc-dc converter was designed to work in continuous conduction mode, although this calculation is beyond the scope of this work.

3.4. Lithium polymer battery model

The battery is a dynamic and nonlinear system with many chemical reactions. Their internal characteristics and circuit parameters change according to the state of charge (SOC). For this reason, in this work, a battery is considered as a power source for the motor instead of an ideal energy source. The hybrid battery model (Fig. 3) is based on a mix of the electrical circuit battery

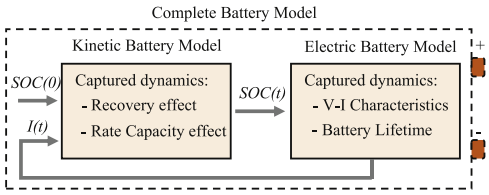

Fig. 3. Lithium polymer battery model.

model and the Kinetic battery model (KiBaM). Its parameters have been identified in [48]. This model was chosen due to its capability to capture nonlinear capacity effects (such as the recovery effect and the rate capacity effect) and also due to its accurate battery SOC tracking and runtime prediction.

The battery delivers the power required for the engine to operate and the voltage and current values at their terminals can be monitored at every moment as well as the battery state of charge (% compared to its maximum load condition). The parameters of the lithium polymer battery are the following: Rhino 3S Lipoly pack, nominal voltage 11.1 *V*, nominal capacity 1050 *mAh*, charge cutoff voltage V_{over} 12.62 *V* and maximum discharge current 20 *C* (21 *A*).

4. Procedure and simulation results

In order to evaluate the performance of the controllers presented in 3.2, several successive simulations (with different simulation times) are carried out with the same reference speed profile. The reference speed profile is a periodic hard step function to fully excite the system's dynamics (see Fig. 4), within the normal working range of the propeller [40]. Each controller (including PID) was adjusted using numerical methods to obtain the lowest possible error control.

Three indicators are computed for each controller at the end of each simulation: (a) The root-mean-square error (RMSE) of the motor speed, (8); (b) An index that includes the energy of the control action, (9), this is similar to the one proposed in [3] (and in many other works); and c) The actual percentage of consumed energy in the battery, (10), which is obtained using the SOC delivered by the battery model.

$$e_\omega = \sqrt{\frac{\sum_{j=1}^{n}\left(\omega(j) - \omega_r(j)\right)^2}{n}} \tag{8}$$

$$J_u = T_s \sum_{j=1}^{n} u(j)^2 \tag{9}$$

$$E_b = 100 - 100 \times SOC(t) \tag{10}$$

$$SOC(t) = SOC_{t_0} - \frac{1}{C_{max}}\left[\int i(t)dt + C_{un}(t)\right] \tag{11}$$

As can be seen in (11), the battery model calculates the SOC according to the delivered electric current, the unavailable charge of the battery $C_{un}(t)$ and the maximum capacity of the battery C_{max} (see [48] for details).

The desired reference speed is repeated until the battery is fully discharged and taken to the extreme of getting 0 *V* at its terminals. It should be noted that the battery voltage should never reach the condition of 0 *V* at their terminals, because this will deteriorate the battery irreversibly. In practice, a limit threshold of 3.3 *V* per cell should be taken into account; so, for the three-cell battery simulated in this paper, the cut-off voltage (COV) should be around 9.9 *V*.

Several simulations of 1800 *s* are carried out. The results of the indicators (8), (9) and (10) for each controller can be observed in Table 1.

Fig. 4 shows the reference and actual speed of the propeller for each controller for the first 30 *s* of simulation, and Fig. 5 shows the corresponding control actions for the same time period. Fig. 6 shows the RMSE for each controller over the entire simulation. Notice that all controllers have an acceptable response with similar speed error.

Next, an analysis is made to compare the classical PID controller with the other controllers. The idea is to get the energy-saving percentage indicated by two saving scores, one based on control efforts using J_u index (SS_{J_u}) and another one based on actual energy delivery by the battery E_b (SS_{E_b}). The reference values are always for the PID controller, and all savings or losses will be referred to the these values.

For the first saving score the index SS_{J_u} is defined taking into consideration (9) applied to the PID controller ($J_{u_{PID}}$) and also to one of the three remaining controllers ($J_{u_{CONT}}$):

$$SS_{J_u} = \frac{J_{u_{PID}} - J_{u_{CONT}}}{J_{u_{PID}}} \times 100 \tag{12}$$

Analogously, for the second saving score the index SS_{E_b} is defined. It considers the actual consumed energy in the battery according to 10 for the PID controller ($E_{b_{PID}}$) and for one of the remaining controllers ($E_{b_{CONT}}$):

$$SS_{E_b} = E_{b_{PID}} - E_{b_{CONT}} \tag{13}$$

In (12) and (13), a null value indicates there is no energy saving or loss between both controllers, positive values indicate the energy saving percentage with respect to the PID controller, and finally; negative values indicate the energy loss percentage with respect to the same PID controller.

With these new index definitions, most of the information given in Table 1 is summarized in Table 2.

As can be seen in Table 2, the Lyapunov based controller consumes up to 14.27% less energy, or 14.16% before the battery reaches the 9.9 *V* practical cut-off voltage (COV), than the PID controller as indicated by the control-effort-based index SS_{J_u}. However, the actual saved energy, which is the energy delivered by the battery, is only up to 1.99% (1.73% considering COV). Similar conclusions can be obtained for the other two controllers. In the case of the sliding mode controller, the saving according to (9) is up to 12.59% (12.53% considering COV), but in terms of the energy delivered by the battery it can be seen that it consumed up to 3.98% more energy than the PID (3.49% considering COV). Finally, in the case of the linear algebra based controller, the saved energy according to SS_{J_u} index is up to 18.14% (18.1% considering COV), but the actual saved energy is only up to 2.96% (2.8% considering COV). All saving scores are shown in Fig. 7a and b for different length simulations.

Analyzing Fig. 7, it can be seen that energy saving percentages are not constant over time. This is because the battery is a finite source of energy and it has its own internal dynamics, thus saving rates are function of the battery state of charge, as shown in Fig. 8. Fig. 7b and Fig. 8 clearly show that saving energy is more sensible to the controller's requirements when the battery reach approximately 15% of its SOC (i.e. when the battery already delivered 85% of its capacity). The sliding mode controller behaves different than the other controllers due to the high frequency content of their associated control law.

Table 1
Time evolution of the Error and Performance Indexes for each controller.

	PID			Lyapunov			Sliding Mode			Linear Algebra		
Time$[s]$	$e_\omega[\frac{rad}{s}]$	$J_u[V^2 s]$	$E_b[\%]$	$e_\omega[\frac{rad}{s}]$	$J_u[V^2 s]$	$E_b[\%]$	$e_\omega[\frac{rad}{s}]$	$J_u[V^2 s]$	$E_b[\%]$	$e_\omega[\frac{rad}{s}]$	$J_u[V^2 s]$	$E_b[\%]$
120	30.915	3975	6.768	30.473	3423	6.659	31.306	3488	6.996	30.597	3272	6.590
240	31.093	7981	13.404	30.664	6891	13.175	31.521	7030	13.888	30.798	6588	13.046
360	31.013	11951	19.978	30.589	10300	19.628	31.441	10499	20.725	30.726	9838	19.436
480	31.095	15990	26.753	30.68	13789	26.281	31.539	14060	27.765	30.812	13175	26.028
600	31.031	19927	33.364	30.619	17173	32.773	31.475	17507	34.640	30.750	16405	32.459
720	31.015	24015	40.275	30.608	20690	39.557	31.462	21085	41.822	30.738	19762	39.179
840	31.077	27956	46.941	30.676	24069	46.103	31.537	24531	48.755	30.805	22990	45.665
960	31.062	32031	53.862	30.667	27563	52.899	31.527	28086	55.947	30.797	26324	52.398
1080	31.112	36005	60.620	30.718	30966	59.538	31.585	31553	62.973	30.846	29574	58.977
1200	31.104	40062	67.531	30.711	34437	66.325	31.578	35083	70.15	30.838	32886	65.702
1320	31.145	44059	74.367	30.748	37863	73.037	31.624	38573	77.251	30.874	36159	72.352
1440	31.137	48086	81.247	30.74	41311	79.794	31.619	42075	84.402	30.863	39448	79.044
1560	31.170	52116	88.180	30.769	44760	86.590	31.662	45586	91.666	30.890	42743	85.774
1580	31.170	52792	89.333	30.768	45326	87.714	31.663	46160	92.899	30.889	43283	86.883
1600	31.167	53453	90.487	30.765	45891	88.838	31.663	46733	94.152	30.886	43822	87.994
1620	31.166	54117	91.654	30.762	46456	89.969	31.666	47306	95.450	30.883	44362	89.110
1640	31.164	54780	92.838	30.760	47022	91.110	31.673	47881	96.822	30.880	44902	90.233
1660	31.170	55493	94.098	30.771	47609	92.310	31.710	48529	98.349	30.891	45458	91.407
1680	31.178	56186	95.395	30.77	48192	93.525	31.848	49149	99.838	30.889	46015	92.594
1700	31.182	56893	96.772	30.771	48775	94.778	32.603	49608	100	30.888	46572	93.808
1720	31.187	57833	98.287	30.774	49365	96.107	-	-	-	30.890	47134	95.078
1740	31.319	59363	99.758	30.781	49955	97.543	-	-	-	30.892	47697	96.416
1760	32.192	61191	100	30.793	50560	99.023	-	-	-	30.900	48259	97.868
1780	-	-	-	30.957	51189	100	-	-	-	30.940	48782	99.255
1800	-	-	-	-	-	-	-	-	-	31.155	49282	100

Battery voltage < 9.9 V Poor controller performance $SOC(t) = 0$

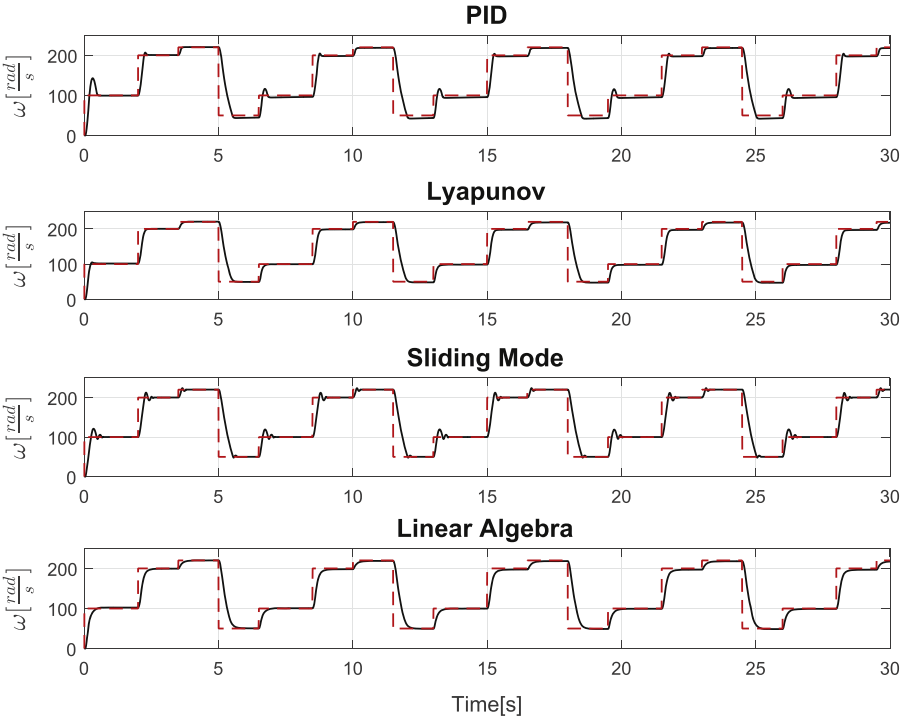

Fig. 4. Properller velocity: references (dotted red/gray) and actual values (solid black) for each controller.

Since the battery is a finite source of energy, the reference speed profile can be followed by the propeller while the battery has enough power. To assess how much time each controller can maintain the propeller working properly, the reference speed is given up to the extreme situation at which the battery voltage reaches 0 *V*. The time period when the controllers begin to malfunction are reproduced in Fig. 9, where the propeller speeds in the last moments for each controller are shown. It can also be noticed that, as expected, these results are in line with the obtained SS_{E_b} index. The time instant at which the system begins to

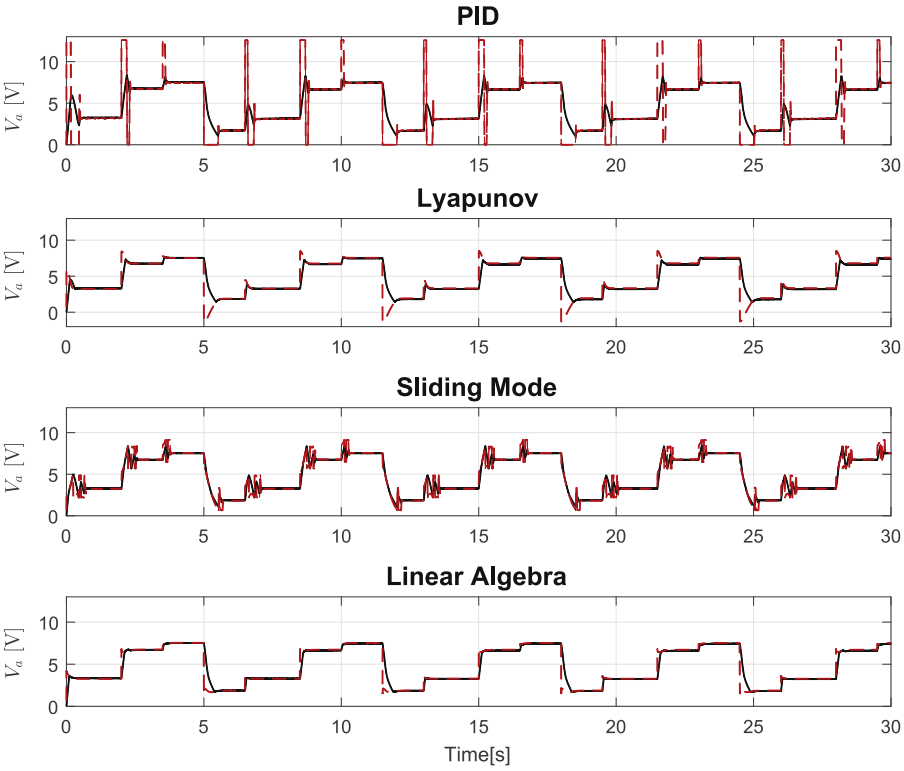

Fig. 5. Control actions for each controller: references (dotted red/gray) and actual values (solid black).

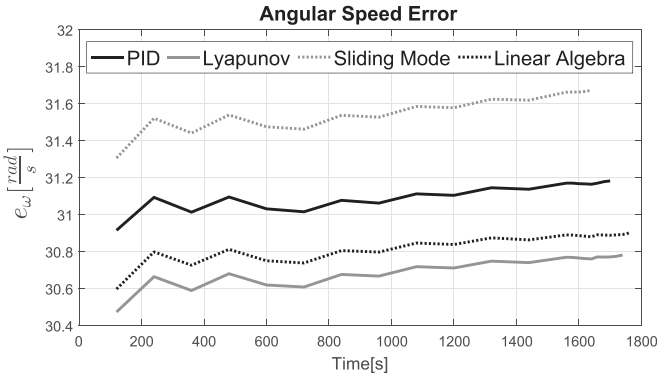

Fig. 6. Angular speed error: time evolution of its root-mean-square value.

malfunction varies with every controller. This time is 1713 *s* for the PID controller, 1746 *s* for the Lyapunov based controller, 1655 *s* for the sliding mode controller and 1765 *s* for the linear algebra based controller. Compared with the PID controller, the Lyapunov and linear algebra based controllers extend the system autonomy by about 1.93% and 3.04% respectively, while the sliding mode controller reduce it by around a 3.39%.

Next, in Fig. 10, it is shown the time evolution of the voltage at the terminals of the battery which is closely linked with the battery state of charge as detailed in [48]. Note that the battery voltage falls exponentially at approximately 85% of their maximum runtime, and this explains why the propeller is suddenly not able to follow the speed reference.

5. Discussion and concluding remarks

Most UAVs currently use electric propulsion and are powered with lithium polymer batteries. Based on this energy-limited scenario, in this work, four well-known control strategies were implemented for a generic UAV propulsion system, including the lithium polymer battery model as the energy source. Numerous simulations were carried out obtaining a quantitative comparison between three advanced model-based control strategies and a classical PID controller. Three indicators and two saving scores were computed to analyze the simulation results.

Conclusions about the energy saving were drawn taking into account the actual consumed energy (SS_{E_b}) and a control-effort-based index (SS_{J_u}), always considering the PID controller as a

Table 2
Controllers' performance with respect to the PID controller.

	Lyapunov		Sliding mode		Linear Algebra	
Time [*s*]	SS_{J_u}	SS_{E_b}	SS_{J_u}	SS_{E_b}	SS_{J_u}	SS_{E_b}
120	13.89	0.11	12.25	− 0.23	17.69	0.18
240	13.66	0.23	11.92	− 0.48	17.45	0.36
360	13.81	0.35	12.15	− 0.75	17.68	0.54
480	13.76	0.47	12.07	− 1.01	17.60	0.73
600	13.82	0.59	12.14	− 1.28	17.67	0.90
720	13.85	0.72	12.20	− 1.55	17.71	1.10
840	13.90	0.84	12.25	− 1.81	17.76	1.28
960	13.95	0.96	12.32	− 2.09	17.82	1.46
1080	14.00	1.08	12.36	− 2.35	17.86	1.64
1200	14.04	1.21	12.43	− 2.62	17.91	1.83
1320	14.06	1.33	12.45	− 2.88	17.93	2.02
1440	14.09	1.45	12.50	− 3.16	17.96	2.20
1560*	14.11	1.59	12.53	− 3.49	17.98	2.41
1580	14.14	1.62	12.56	− 3.57	18.01	2.45
1600	14.15	1.65	12.57	− 3.67	18.02	2.49
1620	14.16	1.69	12.59	− 3.80	18.03	2.54
1640	14.16	1.73	12.59	− 3.98	18.03	2.60
1660	14.21	1.79	–	–	18.08	2.69
1680	14.23	1.87	–	–	18.10	2.80
1700**	14.27	1.99	–	–	18.14	2.96

* Time elapsed before any battery voltage drops below 9.9 V.
** Time elapsed before PID begins to malfunction.

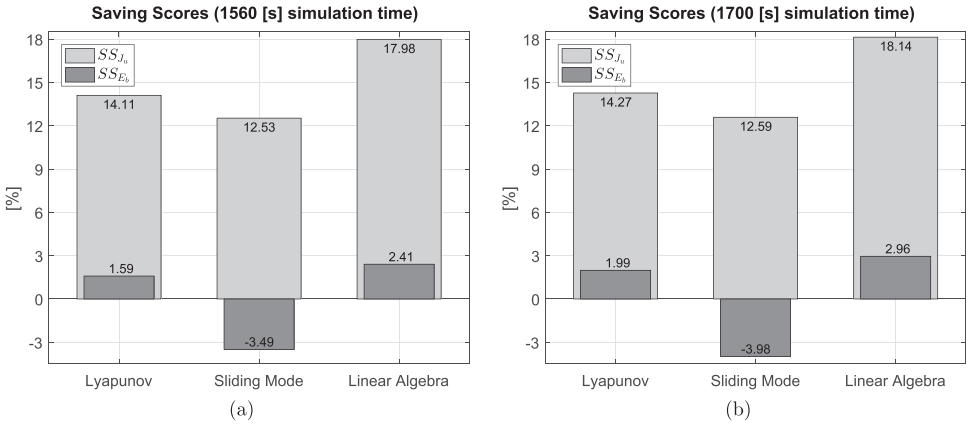

Fig. 7. Energy savings with respect to the PID controller over two different simulations.

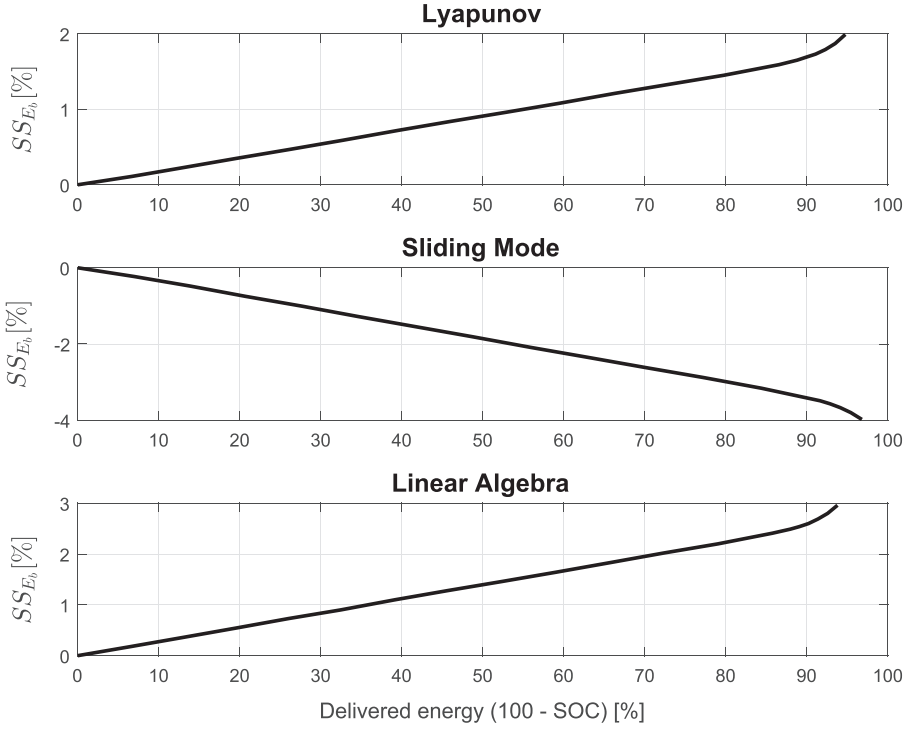

Fig. 8. SS_{E_b} as a function of the battery SOC for each controller.

reference and the battery voltage above the COV. The linear algebra based controller had the best performance in terms of actual energy saving with up to 2.8%, the Lyapunov based controller saved up to 1.73% energy, and finally the sliding mode controller consumed up to 3.49% more energy than the PID controller. On the other hand, according to the control-effort-based index, all three advanced model-based control strategies significantly improved energy savings over the PID controller. The linear algebra based controller, the Lyapunov based controller, and the sliding mode controller saved up to 18.1%, 14.16%, and 12.53% energy respectively.

These results clearly show that it is not possible to reliably conclude about the energy saving analyzing the J_u index (or similar), as it is frequently found in the literature. For instance, if it is decided to apply the sliding mode controller instead of a PID controller based on the saving record of 12.53% provided by the SS_{J_u} index, it would be a mistake from the energy saving point of view.

Furthermore, in spite of the energy saving acquired with the Lyapunov and linear algebra based controllers, these values may not be significant enough in order to justify their implementation, since they are model-based strategies that need a more detailed knowledge of the system. PID controllers do not need a mathematical model of the system and therefore present a great advantage, improving the cost/benefit ratio. Besides, they can be tuned with satisfactory performance in most of the cases.

Certainly, each controller has its own advantages depending on the situation; e.g. the sliding mode controller might be a good option in case of robustness against perturbations were the main objective, even if this imply to spend more energy.

Regarding the increase in propeller operating time, the results are similar to the ones previously mentioned. The linear algebra based controller offers the best performance, increasing about 3% the operating time with respect to the PID controller.

Although the reported energy saving percentages are not significant, they can be more relevant depending on the number of propellers in the UAV (quadrotor, hexacopter, etc.). However, the energy saving ratio is not constant over time but depends on the battery SOC. The controller's performance becomes sensitive as the battery SOC decreases, especially in the range of 85–100% SOC.

In summary, this study has shown that, in order to draw conclusions regarding energy saving for a given low-level controller, it

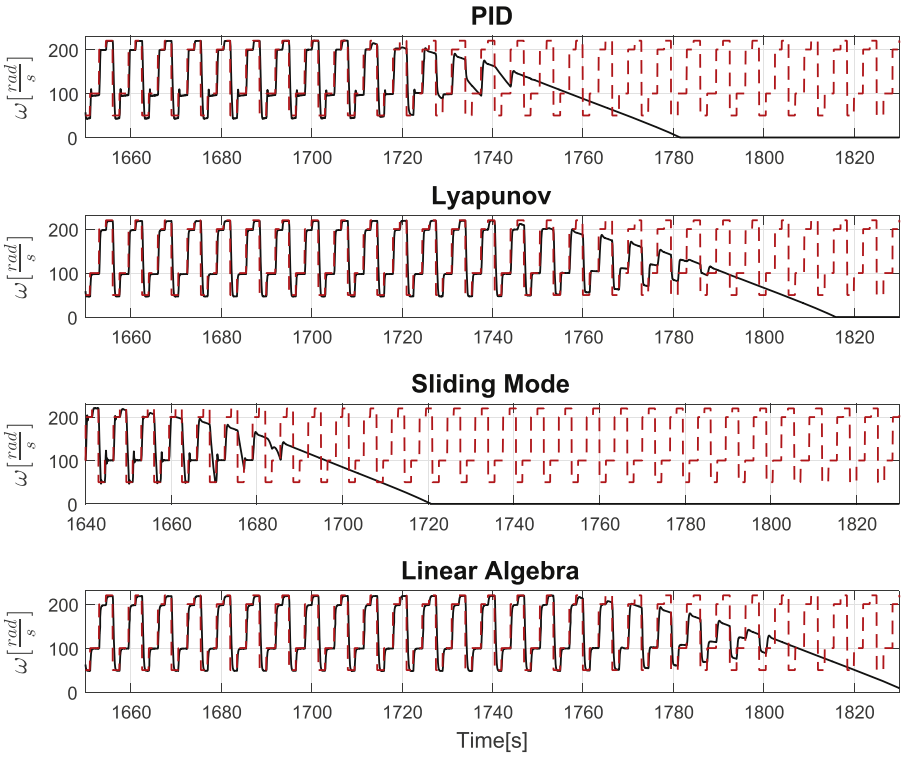

Fig. 9. Propeller speed at the end of maximum runtime for each controller.

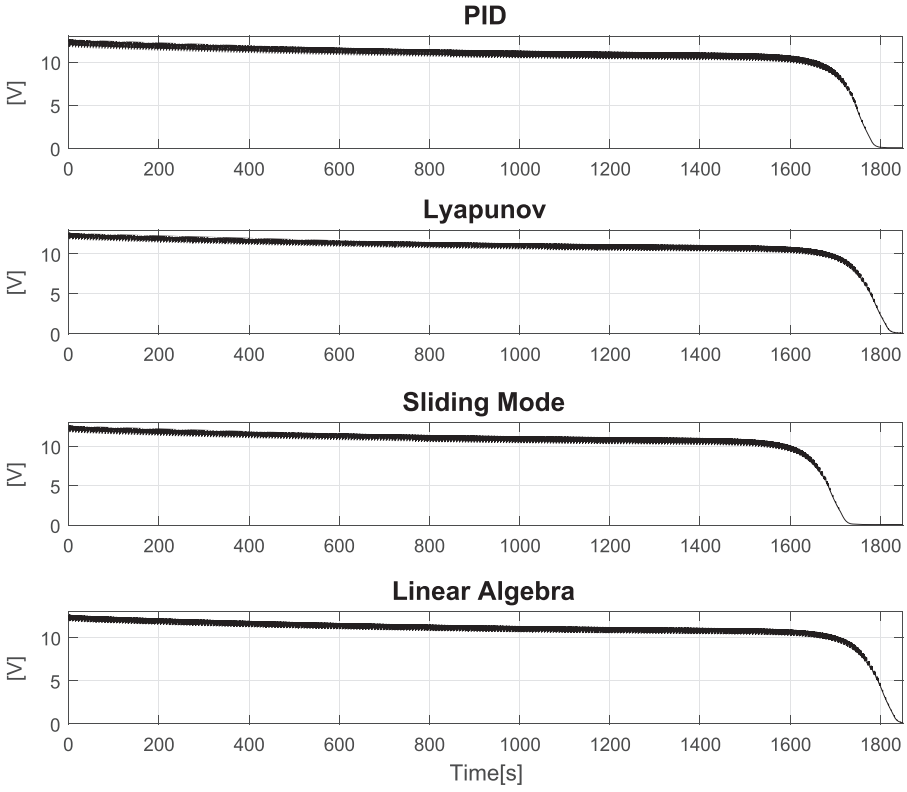

Fig. 10. Battery voltage time evolution for each controller.

is not sufficient to rely on indexes that only consider control efforts. The reason is these control efforts must be delivered by a limited energy source that has its own internal dynamics. Likewise, controllers developed in others control stages should carefully review the conclusions regarding energy savings if they were obtained regardless of the onboard energy source.

Additionally, the propulsion system model parameters depend on the motor type and thus they are not always accurately known. In a future work, a model with uncertainty and more robust controllers will be used to extend these results to a stochastic model and draw broader conclusions.

References

[1] Peng X, Xu D. Intellige nt online path planning for UAVs in adversarial environments. Int J Adv Robot Syst, 9(1) http://dx.doi.org/10.5772/45604.

[2] Liang J. A path planning algorithm of mobile robot in known 3D environment. Procedia Eng 2011;15:157–62.

[3] Chamseddine A, Zhang Y, Rabbath CA, Join C, Theilliol D. Flatness-based trajectory planning/replanning for a quadrotor unmanned aerial vehicle. IEEE Trans Aerosp Electron Syst 2012;48(4):2832–48.

[4] Zhan W, Wang W, Chen N, Wang C. Efficient UAV path planning with multi-constraints in a 3D large battlefield environment, Math. Probl. Eng. Article ID 597092, 12 Pages. http://dx.doi.org/10.1155/2014/597092.

[5] Chakrabarty A, Langelaan JW. Flight path planning for UAV atmospheric energy harvesting using heuristic search. In: Proceedings of the AIAA guidance, navigation, and control conference; 2010.

[6] Dai R, Lee U, Hosseini S, Mesbahi M. Optimal path planning for solar-powered UAVs based on unit quaternions. In: Proceedings of the IEEE conference on decision and control; 2012. p. 3104–09.

[7] Zhang Y, Wu L, Wang S. UCAV path planning by fitness-scaling adaptive chaotic particle swarm optimization. Math. Probl. Eng. Article ID 705238, Pages 9. http://dx.doi.org/10.1155/2013/705238.

[8] Maravall D, de Lope J, Fuentes JP. Vision-based anticipatory controller for the autonomous navigation of an UAV using artificial neural networks. Neurocomputing 2015;151(Part 1):101–7.

[9] Lei X, Lu P. The adaptive radial basis function neural network for small rotary-wing unmanned aircraft. IEEE Trans Ind Electron 2014;61(9):4808–15.

[10] Qu Q, Chen F, Jiang B, Tao G. Integral sliding mode control for helicopter via disturbance observer and quantum information technique. Math. Probl. Eng. Article ID 938246, Pages 7. http://dx.doi.org/10.1155/2015/938246.

[11] Xiong J-J, Zheng E-H. Position and attitude tracking control for a quadrotor UAV. ISA Trans 2014;53(3):725–31.

[12] Zheng E-H, Xiong J-J, Luo J-L. Second order sliding mode control for a quadrotor UAV. ISA Trans 2014;53(4):1350–6 [disturbance Estimation and Mitigation].

[13] Dydek ZT, Annaswamy AM, Lavretsky E. Adaptive control of quadrotor UAVs: a design trade study with flight evaluations. IEEE Trans Control Syst Technol 2013;21(4):1400–6.

[14] Brandão AS, Gandolfo D, Sarcinelli-Filho M, Carelli R. Pvtol maneuvers guided by a high-level nonlinear controller applied to a rotorcraft machine. Eur J Control 2014;20(4):172–9.

[15] Choi YC, Ahn HS. Nonlinear control of quadrotor for point tracking: actual implementation and experimental tests. IEEE/ASME Trans Mechatron 2015;20 (3):1179–92.

[16] Alexis K, Nikolakopoulos G, Tzes A. On trajectory tracking model predictive control of an unmanned quadrotor helicopter subject to aerodynamic disturbances. Asian J Control 2014;16(1):209–24.

[17] Gavilan F, Vazquez R, Camacho EF. An iterative model predictive control algorithm for UAV guidance. IEEE Trans Aerosp Electron Syst 2015;51(3):2406–19.

[18] Akhtar A, Waslander S, Nielsen C. Path following for a quadrotor using dynamic extension and transverse feedback linearization. In: Proceedings of the IEEE conference on decision and control; 2012. p. 3551–56.

[19] Cabecinhas D, Cunha R, Silvestre C. Rotorcraft path following control for extended flight envelope coverage. In: Proceedings of the IEEE conference on decision and control; 2009. p. 3460–65.

[20] Chiou J-S, Tran H-K, Peng S-T. Attitude control of a single tilt tri-rotor UAV system: Dynamic modeling and each channel's nonlinear controllers design. Math. Probl. Eng. Article ID 275905, Pages 6. http://dx.doi.org/10.1155/2013/275905.

[21] Liu Z, Wang Y. Fuzzy adaptive tracking control within the full envelope for an unmanned aerial vehicle. Chin J Aeronaut 2014;27(5):1273–87.

[22] Wu J, Peng H, Chen Q, Peng X. Modeling and control approach to a distinctive quadrotor helicopter. ISA Trans 2014;53(1):173–85.

[23] Santos O, Romero H, Salazar S, Lozano R. Discrete optimal control for a quadrotor UAV: experimental approach. In: Proceedings of the international conference on unmanned aircraft systems; 2014. pp. 1138–45.

[24] Gandolfo D, Rosales C, Patiño D, Scaglia G, Jordan M. Trajectory tracking control of a PVTOL aircraft based on linear algebra theory. Asian J Control 2014;16(6):1849–58.

[25] Rosales C, Gandolfo D, Scaglia G, Jordan M, Carelli R. Trajectory tracking of a mini four-rotor helicopter in dynamic environments – a linear algebra approach. Robotica 2015;33(8):1628–52.

[26] Peng C, Bai Y, Gong X, Gao Q, Zhao C, Tian Y. Modeling and robust backstepping sliding mode control with adaptive RBFNN for a novel coaxial eight-rotor UAV. IEEE/CAA J Autom Sin 2015;2(1):56–64.

[27] Papachristos C, Alexis K, Tzes A. Linear quadratic optimal trajectory-tracking control of a longitudinal thrust vectoring-enabled unmanned tri-tiltrotor. In: Proceedings of the IEEE annual conference on industrial electronics society; 2013. p. 4174–79.

[28] Cabecinhas D, Naldi R, Marconi L, Silvestre C, Cunha R. Robust take-off for a quadrotor vehicle. IEEE Trans Robot 2012;28(3):734–42.

[29] Ryll M, Bülthoff HH, Giordano PR. Modeling and control of a quadrotor UAV with tilting propellers. In: Proceedings of the IEEE International conference on robotics and automation; 2012. pp. 4606–13.

[30] Ryś A, Czyba R, Szafrański G. Practical aspects of trirotor mav development. In: Proceedings of the international micro air vehicle conference summer Ed. Delft University of Technology and Thales; 2011.

[31] Bole B, Teubert CA, Cuong Chi Q, Hogge E, Vazquez S, Goebel K, George V. SIL/HIL replication of electric aircraft powertrain dynamics and inner-loop control for V&V of system health management routines. In: Proceedings of the annual conference of the prognostics and health management society. New Orleans, Louisiana; 2013.

[32] Martínez-Alvarado R, Granda-Gutiérrez EE, Sanchez-Orta A, Ruiz-Sanchez FJ. Modeling and simulation of a propeller-engine system for unmanned aerial vehicles. In: Proceedings of the IEEE international autumn meeting on power electronics and computing; 2013. p. 1–6.

[33] Gebauer J, Kocí P, Sofer P. Multicopter potentialities. In: Proceedings of the international carpathian control conference; 2012. p. 194–97.

[34] Czyba R, Szafranski G. Control structure impact on the flying performance of the multi-rotor VTOL platform – design, analysis and experimental validation. Int. J. Adv. Robot. Syst. 10 (1).

[35] Paw YC, Balas GJ. Development and application of an integrated framework for small UAV flight control development. Mechatronics 2011;21(5):789–802 [special Issue on Development of Autonomous Unmanned Aerial Vehicles].

[36] Stepaniak MJ, Graas FV, Haag MUDe. Design of an electric propulsion system for a quadrotor unmanned aerial vehicle. J Aircr 2009;46(3):1050–8.

[37] Crowther B, Lanzon A, Maya-Gonzalez M, Langkamp D. Kinematic analysis and control design for a nonplanar multirotor vehicle. J Guid Control Dyn 2011;34 (4):1157–71.

[38] Oosedo A, Konno A, Matsumoto T, Go K, Masuko K, Uchiyama M. Design and attitude control of a quad-rotor tail-sitter vertical takeoff and landing unmanned aerial vehicle. Adv Robot 2012;26(3–4):307–26.

[39] Aruneshwaran R, Suresh S, Wang J, Venugopalan TK. Neural adaptive flight controller for ducted-fan UAV performing nonlinear maneuver. In: Proceedings of the IEEE symposium on computational intelligence for security and defense applications; 2013. p. 51–6.

[40] Derafa L, Madani T, Benallegue A. Dynamic modelling and experimental identification of four rotors helicopter parameters. In: Proceedings of the IEEE international conference on industrial technology; 2006. p. 1834–39.

[41] Bouadi H, Bouchoucha M, Tadjine M. Sliding mode control based on backstepping approach for an UAV type-quadrotor. Int J Appl Math Comput Sci 2007;4(1):12–7.

[42] Bouadi H, Cunha SS, Drouin A, Mora-Camino F. Adaptive sliding mode control for quadrotor attitude stabilization and altitude tracking. In: Proceedings of the IEEE international symposium computer and information sciences. Budapest, Hungary; 2011. pp. 449–55.

[43] Lindahl P, Moog E, Shaw SR. Simulation, design, and validation of an UAV SOFC propulsion system. IEEE Trans Aerosp Electron Syst 2012;48(3):2582–93.

[44] Schoemann J, Hornung M. Modeling of hybrid-electric propulsion systems for small unmanned aerial vehicle. In: Proceedings of the AIAA aviation technology, integration, and operations conferences, AIAA/ISSM; 2012. p. 17–9.

[45] Szafranski G, Czyba R, Blachuta M. Modeling and identification of electric propulsion system for multirotor unmanned aerial vehicle design. In: Proceedings of the international conference on unmanned aircraft systems; 2014. p. 470–6.

[46] Khalil H. Nonlinear Systems. 3rd Ed.. Upper Saddle River, NJ: Prentice-Hall; 2002.

[47] Edwards C, Spurgeon S. Sliding Mode Control: Theory and Applications, Series in Systems and Control.London, England: Taylor and Francis; 1998.

[48] Gandolfo D, Brandão A, Patiño D, Molina M. Dynamic model of lithium polymer battery – load resistor method for electric parameters identification. J Energy Inst 2014;88(4):470–9.